Sensing Water Properties at Precise Depths from the Air

John-Paul Ore and Carrick Detweiler

Abstract Water properties critical to our understanding and managing of freshwater systems change rapidly with depth. This work presents an Unmanned Aerial Vehicle (UAV) based method of keeping a passive, cable-suspended sensor payload at a precise depth, with 95% of submerged sensor readings within ± 8.4 *cm* of the target depth, helping dramatically increase the spatiotemporal resolution of water science datasets. We use a submerged depth altimeter attached at the terminus of a 3.5 *m* semi-rigid cable as the sole input to a depth controller actuated by the UAV's motors. First, we simulate the system and common environmental disturbances of wind, water, and GPS drift and then use parameters discovered during simulation to guide implementation. In field experiments, we compare the depth precision of our new method to previous methods that used the UAV's altitude as a proxy for submerged sensor depth, specifically: 1) only using the UAV's air-pressure altimeter; and 2) fusing UAV-mounted ultrasonic sensors with the air-pressure altimeter. Our new method reduces the standard deviation of depth readings by 75% in winds up to 8 m/s. We show the step response of the depth-altimeter method when transitioning between target depths and show that it meets the precision requirements. Finally, we explore a longer, 8.0 *m* cable and show that our depth-altimeter method still outperforms previous methods and allows scientists to increase the spatiotemporal resolution of water property datasets.

1 Introduction

Monitoring shallow surface water systems (< 10 *m*) can be a deep challenge for environmental and water scientists. Hampered by limited boat access, scientists are further constrained because boating and wading mix the water, disturbing the

John-Paul Ore and Carrick Detweiler
Computer Science and Engineering, University of Nebraska-Lincoln, USA e-mail: {jore, carrick}@cse.unl.edu

water properties under investigation. These water properties include temperature, conductivity, dissolved oxygen, and photosynthetically active radiation—all these vary sensitively with small changes in water depth [1]. These stratified properties are linked to ecosystem health and can predict imminent toxic algae blooms that threaten drinking water and fisheries and cost billions of dollars worldwide [2, 3].

Currently, scientists deploy static sensor arrays, often a collection of data-loggers vertically arranged underwater at a static position, and left for days or weeks. Some sensors used by water scientists requiring settling time (often > 3 s), and existing water science datasets from static sensors have ≈ 0.25 m resolution in depth [4]. These static sensors yield datasets with good temporal resolution, but are limited by poor spatial resolution because they have to be installed separately at each location. To increase the spatiotemporal resolution, our prior work presented the first UAV-based water sampler [5], followed subsequently by several efforts [6, 7, 8, 9, 10, 11, 12]. The UAV flies above water while connected by cable to a sensor payload below water, as shown in Figure 1. Our follow-on work [13] explored *in-situ* water sensing at different depths with a UAV-based submerged sensor payload, and found it does not cause mixing for temperature. However, in this follow-on work the UAV's air pressure altimeter caused the submerged sensor to wander up and down around the target depth, limiting precision.

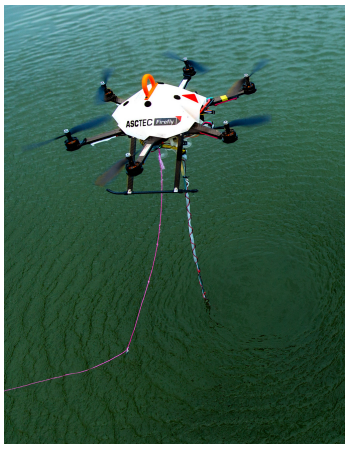

Fig. 1: UAV-system with a passive cable and sensors for measuring water properties at precise depths.

To increase the depth precision of water science datasets, this paper proposes and experimentally evaluates using a depth altimeter as input to a controller that seeks to minimize the target depth error using only the UAVs motors. We assume calm waters ('lentic', not flowing) and that the UAV is stationary. This is challenging because the semi-rigid cable between the UAV and the submerged depth altimeter exhibits non-linear dynamics when bending and descending in water. Fortunately, these depth sensors are fast (50 Hz), light ($< 5g$), and precise (± 3 mm), and are already included in many underwater sensor payloads. We first explore the feasibility of this approach in simulation including wind and water, then use parameters discovered in simulation to guide implementation, and finally test the implementation of our method in field experiments.

Our contributions are:

- A new method to maintain a precise depth for a submerged sensor payload while passively connected by cable to a UAV. We use only a lightweight submerged depth altimeter, reducing the standard deviation of target depth errors from 16.1 cm to 4.2 cm compared with the next best method. This method enables increased spatiotemporal resolution of water science datasets without additional payload.

- Field tests of this depth-altimeter method, with comparisons to two previous methods: 1) air pressure altimeter alone; and, 2) air pressure fused with ultrasonic rangefinders. We compare these approaches using a 3.5 *m* cable for water depths down to 2.5 *m*, showing an reduction of target depth error by 75%.
- An initial exploration of using an 8.0 *m* cable, showing sufficient precision for sensing at greater depths.

2 Related Work

Previous efforts relate to our current work in several ways: either a UAV is used to measure water properties, or autonomous surface / underwater vehicles (ASVs and AUVs) are used to measure water properties, or a UAV makes a pose and altitude estimation in unknown environments, or a UAV has a cable-suspended load.

Several efforts seek to use UAVs to monitor water properties [6, 7, 8, 9, 10, 12]. These systems use air pressure altimeters to estimate altitude, and like these efforts we seek to sense water properties with a cable-connected payload, but unlike these works we focus on precisely controlling the depth of the sensor payload. Systems like the fixed-wing Flying Fish [14] maintain persistent observation of surface properties, but cannot detect subsurface properties. Some efforts seek an amphibious UAV [15], and like this work we are interested in the advantages offered by UAVs to water monitoring, but unlike this work we seek to minimize water column mixing, that can take hours to settle. Our previous work presents evidence that sensing by a small, submerged sensor payload (≈ 2 *cm* diameter sensor, 1 *cm* cable) does not cause a mixing disturbance that impacts water temperature measurements [13].

In environmental monitoring, Dunbabin [16] uses multiple ASVs to sample greenhouse gasses, while underwater the MARES AUV system samples water quality for long duration at depths up to 100 *m* [17]. Zhang *et al.* [18] explore water columns with a gliding, fish-like robot, and Higgin's *et al.* [1] WaterBug descends passively in a water column to collect a single water sample at a target depth. Unlike these systems, we want to quickly deploy and redeploy to disconnected or difficult to reach water bodies.

Several approaches seek to estimate altitude for micro UAVs in unstructured outdoor environments, including Jain *et al.* [19], who autonomously explored rivers using specular laser returns to estimate the plane of the river surface. Unlike this work we seek a method that minimizes the payload devoted to non-water-property sensing. Burri *et al.* [20] use a stereo camera and IMU to map and estimate a pose in a previously unknown environment, but these methods have not been demonstrated over water, to our knowledge. Our previous work [7] explores the use of fusing downward-facing ultrasonic sensors with an air pressure altimeter, and we use this method for comparison in the current work.

Several efforts model and control cable-suspended payloads from a UAV [21, 22], and assume that the cable can be observed. We likewise use a cable-suspended payload, but do not attempt to observe the cable during flight.

3 Technical Approach

This section describes our approach to the problem of obtaining precise depth control of a submerged sensor payload with minimal system complexity while retaining the benefits of monitoring water properties by UAV. Based on our experience, we assumed that the biggest obstacles would be non-linear dynamics of the partially submerged cable and transient lateral disturbances from wind and GPS drift. But we also wondered about the impact of signal delay in measuring and transmitting depth readings before the controller can use them. We start by developing a model for how the cable-connected sensor moves in the water, and then explore the feasibility and initial parameters in simulation.

3.1 System Model and Simulation to Explore Feasibility

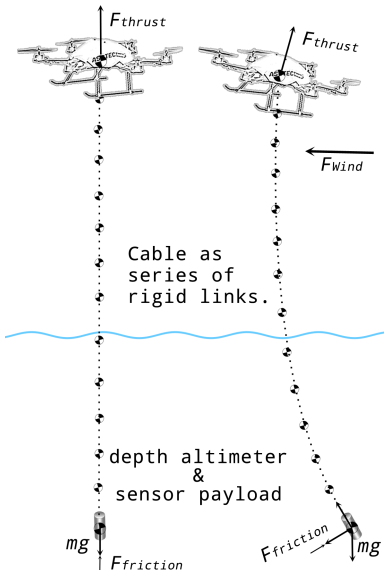

Fig. 2: Model of UAV-system hovering over still water, showing the suspended cable as a series of rigid links. The left side of the figure shows the ideal case, the right shows the system during a lateral disturbance from wind.

Figure 2 shows the UAV modeled as a point mass and the cable as a series of rigid links, following the approach in [22]. We use Simulink for two configurations, a ideal and perfectly vertical case, and a laterally disturbed case to model wind and GPS drift.

Modeling the Ideal Case. In the ideal case, the cable is vertical and all forces are parallel to gravity, as the UAV, cable, and depth altimeter move up and down. When the UAV moves up, the sensor payload is directly coupled. When the UAV moves down, the only forces acting on the payload are gravity and resistance from water. The resistance from water limits the sensor's descent rate to slower than the UAV.

To model the descent rate, we started by experimentally determining the terminal velocity of the sensor in water. We released the sensor at the top of a translucent 3 m vertical water test tank (≈ 25 cm radius by 4 m tall) and measured the time at which the sensor reached markings of depth 1 m and 2 m. Using six observations, we estimate the average terminal velocity, v_t, to be 0.54 m/s. Then, using the terminal velocity equation:

$$v_t = \sqrt{\frac{2mg}{\rho A C_d}} \tag{1}$$

we calculate the constant ρAC_d, where ρ is the density of water, A is the area in the direction of the movement, and C_d is the drag co-efficient. Using this constant with the mass of the sensor, m, and gravity, g, we solve for the resistive force as a function of velocity:

$$F_{friction} = \frac{1}{2}\rho AC_d v^2 \tag{2}$$

We use $F_{friction}$ from Equation 2 to model how the sensor will descend in water. In simulation, $F_{friction}$ limits the descent velocity of the senor payload as well as making it drag against lateral disturbances. Decreasing the target depth by < 1 m allows the submerged sensor to descend fast enough to match the descent of the UAV. Decreasing the target depth by > 1 m requires limiting the descent velocity of the UAV to avoid the UAV outpacing the submerged sensor.

Modeling Lateral Disturbances. Figure 2 also shows the lateral disturbance case from wind or GPS drift. We want to model wind and GPS drift because we believed lateral disturbances could be a critical impediment to our approach.

To model lateral disturbances, we are inspired by the U.S. Military Wind Gust Model [23], that uses a sigmoid function that 'ramps up' a gust over time. We model wind as the sum of two smoothed random number sequences that are directly added to the forces exerted on the UAV in x and y. The two sequences operate at different time scales, one changing every second and at a small scale, and the other changing every 15 seconds at a larger scale. Overall, a maximum force of 0.08 N tends to 'blow the system off course' by about 1-2 m, consistent with field observation. Note that during lateral disturbances, $F_{friction}$ acts on the submerged sensor payload and opposes the translation. The simulation indicates that the UAV-cable-sensor system remains stable in response to lateral disturbance while controlling depth using the depth altimeter with the UAV motors. We leave the detailed discussion and analysis of this for future work.

Modeling Signal Delay and Sampling Frequency. We model signal delay because of the multiple network hops for depth readings: from depth altimeter to embedded system to control computer and back to the UAV (as shown in Figure 3). In simulation, a signal delay of less than 100 ms was required to ensure that the system converges smoothly to changes in target depth of ≈ 1 m, with smaller signal delay yielding only modest improvements.

We model the sampling rate of the depth altimeter to find a baseline requirement, and find that at least 10 Hz is required. During simulation, the system could still converge to a target depth with a slow sampling rate of 1.25 Hz and a long delay of 700 ms, but with significant oscillations.

Key simulation results:

- Depth altimeter sampling frequency $>$ 10 Hz.
- Signal delay from the depth altimeter to UAV control input $<$ 100 ms.
- Small transient lateral disturbances do not cause the system to become unstable.
- Limit UAV descent velocity or limit change in target depths to $<$ 1 m.

We now use these simulation results to guide our implementation.

4 Implementation Details

This section describes the system architecture, depth altimeter characterization, and descriptions of the three flight modes under test.

4.1 System Architecture

Figure 3 shows the system architecture used during experiments, consisting of: 1) AscTec Firefly hexrotor UAV; 2) two embedded systems; and, 3) a control computer.

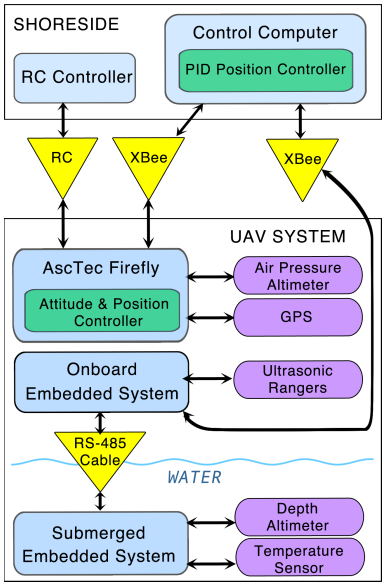

Fig. 3: System Architecture.

The Firefly includes a GPS and air pressure altimeter as well as an on-board controller for attitude and position. We chose the Firefly for overwater experiments because it can return to shore even after one motor fails. It has a payload capacity of 600 g, flies for 15-20 minutes per battery, and tolerates winds up to 10 m/s.

The sensor payload installed on the Firefly consists of two embedded systems, the first installed on the vehicle and the second waterproof system attached to the end of the cable that dangles below the UAV. The first embedded system has an NXP-LPC2368 (ARM7TDMI) microprocessor running a control loop at 50 Hz, and has inputs for a variety of water sensors and is used to log and transmit real-time readings over radio. The submerged embedded system contains an ATmega-1284pb microprocessor that reads the depth altimeter at 50 Hz. The embedded system installed on the UAV receives the depth readings and re-transmits them to the control computer. The control computer is an Apple Macbook "Early 2015" running Ubuntu 14.04 with ROS Jade for control and logging.

In this architecture, we estimate the complete signal delay from the depth altimeter to the UAV control input to be 45 ms worst case, within the 100 ms bound identified during simulation and described in Section 3.1.

4.2 Depth Altimeter Characterization

For the depth altimeter, we use a Measurement Specialties MS5803-01BA [24] installed on an embedded system, and shown in Figure 4. By the datasheet, this sensor is water resistant to 100 m with a built-in 24-bit ADC and a 10 ms response time, plus an additional 10 ms to read the onboard thermometer to correct for temperature variation. The 20 ms total means a maximum sampling frequency of 50 Hz, well above the baseline 10 Hz indicated by simulation.

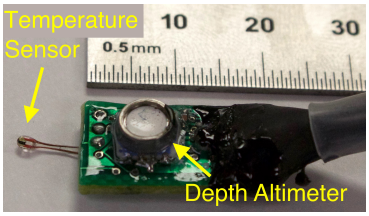

Fig. 4: The waterproof embedded system and sensor payload.

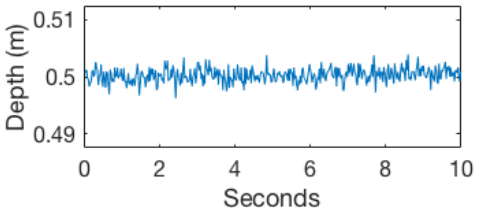

Fig. 5: Depth altimeter steady state error at constant depth showing ± 3 *mm* error.

To characterize the depth altimeter's steady-state error, we placed it at a fixed depth in a bucket of 22°C water. Figure 5 depicts 10 *s* of readings, and shows steady-state error of ± 3 *mm*. We characterized and corrected for the depth sensor's bias using the vertical tank described in Section 3.1. Because of the MS5803's fast response, accuracy to depths of 10 *m*, and small steady-state error, we use this sensor for comparison during our field experiments.

Note that changes to ambient air pressure causes pressure changes in water, impacting depth readings. For example, an air pressure difference of 100 *mbar* across a strong weather front results in 0.6 *m* pressure difference measured in water depth. In practice, the depth altimeter must be calibrated for the current air pressure every few hours by submerging the sensor to a known depth (we used 5 *cm*). However, during a 20-minute flight, the total air pressure change is likely small, and transient air pressure fluctuations like wind that cause an air altimeter change of ± 2 *m* cause a depth altimeter change of only ± 3 *mm*. This makes sense since water is ≈ 800 times denser than air.

4.3 Flight Modes: Depth, Air Pressure, Ultrasonic + Air Pressure

We implement three flight modes: depth altimeter, air pressure altimeter, and ultrasonic altimeter. The depth altimeter mode is the new method proposed and implemented in this work, and the air pressure and ultrasonic modes are alternative methods for comparison during experiments. Note that the depth altimeter method controls depth while air pressure and ultrasonic methods control the UAV's altitude as a proxy for sensor depth.

Depth altimeter mode controls only thrust, while the UAV controls roll, pitch, and yaw. On the control computer, the stream of depth readings is passed through a Kalman filter assuming Gaussian noise (characterized in Section 4.2), and we assume a linear state transition function during hover. The filtered readings are used in a 50 Hz PID position controller for depth that commands thrust.

Air pressure altimeter mode uses the UAV's onboard controller for everything: roll, pitch, thrust, and yaw. Air pressure mode uses the UAV's air pressure altimeter, GPS, and an onboard IMU together to create a fused pose estimate. This is the basic 'out-of-the-box' controller.

Ultrasonic altimeter mode fuses downward-facing ultrasonic sensors with the air-pressure altimeter to form an altitude estimate. To prevent the ultrasonic sensors from seeing the cable, the readings from each of the two ultrasonic sensors are pre-filtered based on both the variance of recent readings and the proximity of readings to the current altitude estimate, before being passed through a Kalman filter. The details of this pre-filtering are described in previous work [7].

Now that we have an implementation guided by simulation, we discuss experimental validation in the field.

5 Field Experiments

This section describes the setup of field experiments and presents results. To test our approach, we designed three field experiments: 1) a comparison of depth precision for three flight modes with a 3.5 m cable and submerged sensor payload; 2) step responses to changes in target depth for the proposed depth altimeter method; and, 3) an initial exploration of the depth altimeter method using a longer, 8.0 m cable, measuring precision and step response.

All field experiments were conducted during March 2017 at Wildwood Lake near Lincoln, Nebraska, USA, as shown in Figure 6. In total, we flew 33 missions. The comparison dataset was collected during three days and the wind average speeds were 3.5 m/s, 2.0 m/s, and 1.3 m/s, respectively with maximum 5-second wind speed of 8.5 m/s, 7.2 m/s, and 7.9 m/s, respectively, indicating occasional strong gusts. We measured wind speed and direction using a weather station recording into a time-synced computer log.

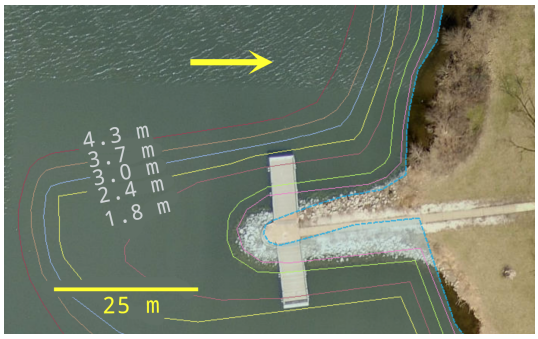

Fig. 6: Wildwood Lake near Lincoln, Nebraska, USA, shown with depth contours. The yellow arrow indicates location of field experiments. Map courtesy of Nebraska Game & Parks.

5.1 Comparison of Flight Modes for Maintaining Constant Depth.

The purpose of this experiment is to compare three flight modes and quantify how precisely we can maintain the depth of a sensor payload. The three modes are detailed in Section 4.3.

We launched the vehicle from a jetty to a sampling location 10 m from shore, indicated in Figure 6. For these experiments we used a 3.5 m cable affixed below

the UAV's center of mass. For each mission, we flew to the sampling location by human pilot, descended until the depth altimeter was at least 1 m deep, then switched to one of the computer controlled flight modes. Once in computer control mode, the system attempts to remain stationary in x and y while recording depth. We flew two modes per flight, each for ≈ 4 minutes. It can be difficult to compare the results of different outdoor trials, so within a single flight we tested different flight modes successively, and recalibrated the depth altimeter every few hours to adjust for changing air pressure. We swapped the flight mode sequence between trials to ensure that no mode benefited from fresher batteries. In total, we flew 12 minutes maintaining a specified depth for each mode. We use the depth altimeter reading for comparison, as it is accurate and fast as described in Section 4.2, and use this as a basis for evaluating the target depth precision.

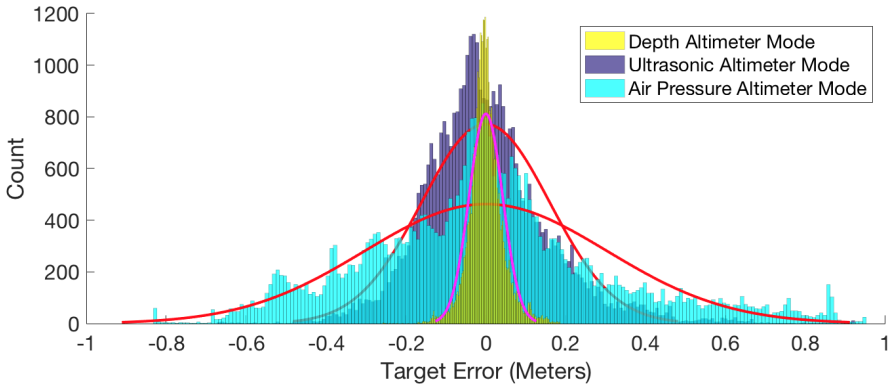

Fig. 7: Distribution of target depth error during three flight modes.

Figure 7 show the results of comparing depth precision during the three flight modes. The data are collated from 3-4 flights per mode. We assume a Gaussian distribution of target depth errors and estimate the standard deviation σ with Matlab's `normfit` function. As shown in the figure, the depth altimeter mode is significantly more precise than either ultrasonic or air pressure modes. Specifically, the statistical dispersion of depth readings in depth altimeter mode keeps 95% of readings within ± 8.4 $cm (\sigma = 4.2$ $cm)$, two standard deviations from the target depth. This is within our goal of being able to obtain readings with a resolution of at least ≈ 25 cm. The ultrasonic-pressure altimeter mode shows $\sigma = 16.1$ cm, or 95% of readings within ± 32.2 cm of the target depth, while the air altimeter has the largest dispersion, with 95% of readings within ± 60.2 cm ($\sigma = 30.1$ cm).

To better show the variation of depth readings in each mode, Figure 8 shows examples of 4 minutes of continuous flight for each mode along with the 5-second-average wind speeds. As shown in Figure 8(a), depth altimeter mode stays closest to the target depth with almost no drift and small disturbances, and note than it maintained this target depth during 5 m/s wind gusts. Also note in Figure 8(b) how

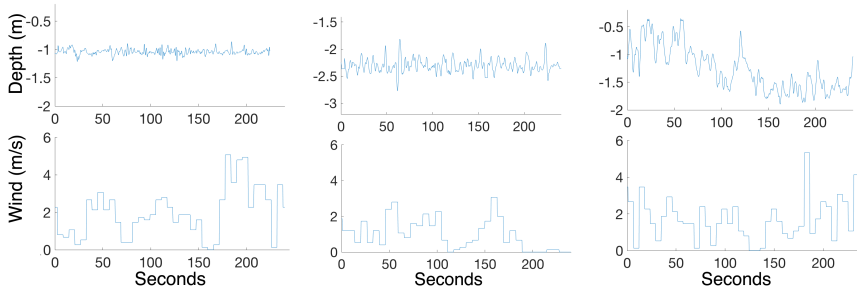

(a) Depth altimeter mode (b) Ultrasonic altimeter mode (c) Air altimeter mode

Fig. 8: Comparison of depth precision using three different flight modes with 5-second-average windspeeds. Note that the y-axes of all depth figures span 1.8 m.

ultrasonic altimeter mode is not as precise and occasionally deviates almost a meter even with calmer winds, but does not drift significantly over time, unlike the air pressure altimeter mode. During the ultrasonic altimeter test, we moved the UAV closer to the water so that the ultrasonic rangefinders could get better readings, resulting in greater depth compared to the other two methods. In Figure 8(c), the air altimeter mode depth readings change by $30-40$ cm in a small amount of time, but that within two minutes the depth readings can be off by ± 0.75 m. The large drift in air pressure mode is likely caused by larger changes in ambient air pressure, like wind.

5.2 Step Response of Depth Altimeter Mode for a 3.5 m *Cable*

To determine if the system under depth altimeter control could transition between target depth reference points, we conduct 'step response' maneuvers. Figure 9 shows the step responses under depth altimeter control. For each reference depth, we set the system to hold a particular target depth, then adjust the target by 0.5 m. Notice how the reference depths are repeatable both ascending and descending and the depth quickly settles to within ± 5 cm of the target depth. For comparison, Figure 10 shows the step response for air pressure altimeter mode. We do not show the step response for ultrasonic altimeter mode because it only works well when close to the water. We use 0.5 m changes to avoid the UAV outpacing the submerged sensor toward the target depth, until we implement a descent velocity limit, reserved for future work.

5.3 Longer 8.0 m *Cable: Target Error and Step Response*

As an additional experiment, we extended the cable length to 8.0 m. The reason we are interested in a longer cable is that in some applications we want to be able

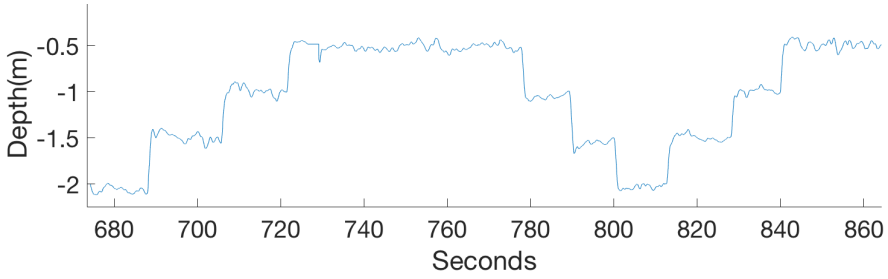

Fig. 9: Step response of depth altimeter mode at 0.5 *m* increments for a 3.5 *m* cable.

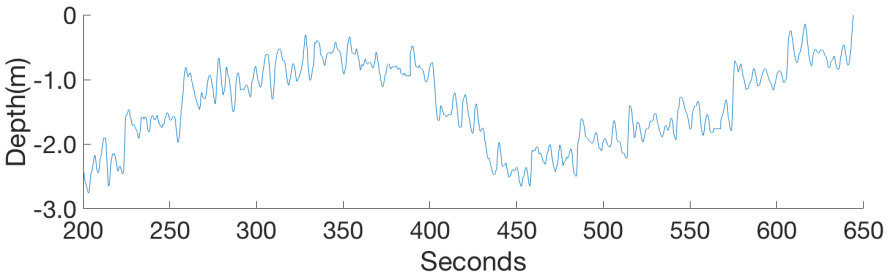

Fig. 10: Step response of air pressure altimeter mode at 0.5 *m* increments for a 3.5 *m* cable.

to measure water properties across a range of depths, nearly all < 10 *m*, and we also wanted to see what impact a longer cable would have on the ability to control the depth. Therefore, we field tested the depth altimeter flight mode with the 8.0 *m* cable. The experimental setup is identical to the depth altimeter mode tests in Sections 5.1-5.2 other than the longer cable length. We were only able to test the 8.0 *m* cable down to a depth of ≈ 4 *m*, due to depth limitations at our field location.

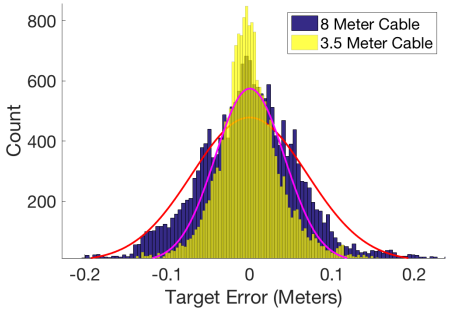

Fig. 11: Target depth error comparison between 8.0 *m* and 3.5 *m* cables both using depth altimeter mode over 4 minutes of flight.

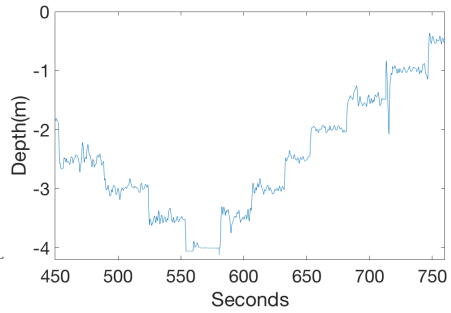

Fig. 12: Step response to target depths at 0.5 *m* increments for an 8.0 *m* cable. Note the flat readings near 550 seconds indicating the water bottom.

Figure 11 shows the results for holding a target depth, and for comparison the figure shows the distribution of target errors for the 3.5 m cable depth altimeter experiments of Section 5.1. As shown in the figure, the 8.0 m cable is less precise than the 3.5 m cable, with 95% of readings within ± 14 $cm(\sigma = 7.0\ cm)$, still close to the desired ≈ 0.25 m resolution. The dispersion of target errors for the 8.0 m cable still improves on the ultrasonic and air-pressure altimeter modes, even when those modes use the shorter 3.5 m cable.

Figure 12 shows the step response between target depths at 0.5 m increments. Like the system with the 3.5 m cable under depth altimeter control, the configuration with an 8.0 m cable can transition precisely between target depths.

Because the 8.0 m cable allows the sensor payload to remain within ± 14 cm for nearly all readings, this means an 8.0 m cable might be viable for monitoring water properties down to a depth of 7 m, and we intend to explore this in future work.

6 Discussion and Future Work

The precision for the depth altimeter flight mode exceeded our expectations, especially while flying in wind gusts at 80% of the manufacturer's limit of 10 m/s. We believe that controlling depth with a depth altimeter and the UAVs motors will enable dramatically better vertical resolution with the advantages of quick deployment and redeployment by UAV without additional sensors.

One future challenge includes integrating sensor payloads requested by water scientists. The challenge is that the irregular shapes and configurations of sensors might result in different drag and terminal velocities.

Fusing altitude and depth data might appear to be natural course, but we see little advantage in fusing because other sensors measure the UAV's altitude, not the depth of the sensor payload. A hybrid controller could switch between flight modes based on violations of invariants inferred during successful flights [25] (like hitting the bed below the water, becoming entangled, or getting encased in muck).

We examined the depth error as a function of lateral disturbance (error in x and y position), like when wind or GPS drift pushes the UAV out of position. However, we saw no relationship between lateral error and depth error. We plan to explore this in flowing water ('lotic systems') or while the UAV is translating.

Flying over water with micro UAVs that are not waterproof is inherently risky, and there are a number of ways to increase the reliability of this kind of system: 1) better protection from unsafe descent, including conductivity sensors on the cable near the UAV, and at least one ultrasonic sensor for redundant backup; 2) breakaway cable with a buoy; 3) a protective cover for the depth altimeter to prevent fouling; and, 4) buoyancy of the UAV.

7 Conclusions

This work explores a novel method for precisely maintaining the target of a submerged sensor payload passively cabled to a UAV. Our method enables 95% of sensor payload readings within ± 8.2 *cm* of the target depth, increasing the depth resolution of UAV-based water property datasets. We tested our method in the field moderately windy conditions ($4-8$ m/s) and the system still quickly and accurately reached and maintained target depths. The non-linear dynamics of a system with a semi-rigid cable are challenging to model as it interacts with wind and water. Still, we used simulation to guide and refine our approach before implementation. We conducted field experiments that validate the approach, resulting in a 75% reduction in standard deviation from a target depth when compared to the previous best method. We also presented initial results for a longer, 8.0 *m* cable, the longest cabled sensor system yet attempted in UAV-based sub-surface water monitoring, and demonstrated that even an this length the approach allows water monitoring at precise depths from the air.

Acknowledgements Thanks to Dr. Sebastian Elbaum and Dr. Justin Bradley for insightful discussions. Becca Horzewski helped design and build the underwater sensor. For help with field experiments we thank Ajay Shankar, Ashraful Islam, Adam Plowcha, Chandima Fernando, and Nishant Sharma. This work partially supported by NSF NRI-1638099, USDA-NIFA 2013-67021-20947 and USDA-NIFA 2017-67021-25924.

References

1. J. Higgins and C. Detweiler, "The Waterbug sub-surface sampler: Design, control and analysis," in *2016 IEEE/RSJ International Conference on Intelligent Robots and Systems (IROS)*, 2016, pp. 330–337.
2. W. K. Dodds, W. W. Bouska, J. L. Eitzmann, T. J. Pilger, K. L. Pitts, A. J. Riley, J. T. Schloesser, and D. J. Thornbrugh, "Eutrophication of U.S. freshwaters: Analysis of potential economic damages," *Environmental Science & Technology*, vol. 43, no. 1, pp. 12–19, Jan. 2009.
3. I. Sanseverino, D. Conduto, P. POZZOLI, S. Dobricic, and T. Lettieri, "Algal bloom and its economic impact," *EUR 27905 EN; doi: 10.2788*, vol. 660478, 2016.
4. H. B. Fischer, J. E. List, C. R. Koh, J. Imberger, and N. H. Brooks, *Mixing in inland and coastal waters*. Elsevier, 2013.
5. J. P. Ore, S. Elbaum, A. Burgin, B. Zhao, and C. Detweiler, "Autonomous aerial water sampling," in *Proc. of The 9th Intl. Conf. on Field and Service Robots (FSR). Brisbane, Australia*, vol. 5, 2013, pp. 137–151.
6. M. Schwarzbach, M. Laiacker, M. Mulero-Pazmany, and K. Kondak, "Remote water sampling using flying robots," in *2014 International Conference on Unmanned Aircraft Systems (ICUAS)*, 2014, pp. 72–76.
7. J. P. Ore, S. Elbaum, A. Burgin, and C. Detweiler, "Autonomous aerial water sampling," *Journal of Field Robotics*, vol. 32, no. 8, pp. 1095–1113, 2015.
8. P. Rodrigues, F. Marques, E. Pinto, R. Pombeiro, A. Lourenço, R. Mendonça, P. Santana, and J. Barata, "An open-source watertight unmanned aerial vehicle for water quality monitoring," in *OCEANS'15 MTS/IEEE Washington*, 2015, pp. 1–6.

9. J. H. Bae, E. T. Matson, and B.-C. Min, "Towards an autonomous water monitoring system with an unmanned aerial and surface vehicle team," in *Safety, Security, and Rescue Robotics (SSRR), 2015 IEEE International Symposium on*, 2015, pp. 1–2.
10. M. Ribeiro, A. S. Ferreira, P. Gonçalves, J. Galante, and J. B. de Sousa, "Quadcopter platforms for water sampling and sensor deployment," in *OCEANS 2016 MTS/IEEE Monterey*, 2016, pp. 1–5.
11. C. Koparan and A. B. Koc, "Unmanned aerial vehicle (uav) assisted water sampling," in *2016 ASABE Annual International Meeting*. American Society of Agricultural and Biological Engineers, 2016, p. 1.
12. A. DeMario, P. Lopez, E. Plewka, R. Wix, H. Xia, E. Zamora, D. Gessler, and A. P. Yalin, "Water plume temperature measurements by an unmanned aerial system (UAS)," *Sensors*, vol. 17, no. 2, p. 306, 2017.
13. M. Chung, C. Detweiler, M. Hamilton, J. Higgins, J. P. Ore, and S. Thompson, "Obtaining the thermal structure of lakes from the air," *Water*, vol. 7, no. 11, pp. 6467–6482, 2015.
14. R. Eubank, E. Atkins, and D. Macy, "Autonomous guidance and control of the Flying Fish ocean surveillance platform," in *AIAA Infotech@ Aerospace Conference*, 2009, pp. 2009–2021.
15. D. Bershadsky, S. Haviland, P. E. Valdez, and E. Johnson, "Design considerations of submersible unmanned flying vehicle for communications and underwater sampling," in *OCEANS 2016 MTS/IEEE Monterey*, 2016, pp. 1–8.
16. M. Dunbabin, "Autonomous greenhouse gas sampling using multiple robotic boats," in *Field and Service Robotics*. Springer, 2016, pp. 17–30.
17. N. A. Cruz and A. C. Matos, "The MARES AUV, a modular autonomous robot for environment sampling," in *OCEANS 2008*, 2008, pp. 1–6.
18. F. Zhang, O. En-Nasr, E. Litchman, and X. Tan, "Autonomous sampling of water columns using gliding robotic fish: Control algorithms and field experiments," in *2015 IEEE International Conference on Robotics and Automation (ICRA)*, 2015, pp. 517–522.
19. S. Jain, S. Nuske, A. Chambers, L. Yoder, H. Cover, L. Chamberlain, S. Scherer, and S. Singh, "Autonomous river exploration," in *Field and Service Robotics*. Springer, 2015, pp. 93–106.
20. M. Burri, H. Oleynikova, M. W. Achtelik, and R. Siegwart, "Real-time visual-inertial mapping, re-localization and planning onboard mavs in unknown environments," in *2015 IEEE/RSJ International Conference on Intelligent Robots and Systems (IROS)*, 2015, pp. 1872–1878.
21. S. Tang and V. Kumar, "Mixed integer quadratic program trajectory generation for a quadrotor with a cable-suspended payload," in *2015 IEEE International Conference on Robotics and Automation (ICRA)*, 2015, pp. 2216–2222.
22. F. Goodarzi, D. Lee, T. Lee *et al.*, "Geometric stabilization of a quadrotor UAV with a payload connected by flexible cable," in *American Control Conference (ACC), 2014*, 2014, pp. 4925–4930.
23. *FLYING QUALITIES OF PILOTED AIRPLANES*, U.S. Military, 11 1980.
24. "Pressure Sensor MS5803-01BA," http://www.te.com/usa-en/product-CAT-BLPS0038.html, Accessed: 2017-3-21.
25. H. Jiang, S. Elbaum, and C. Detweiler, "Inferring and monitoring invariants in robotic systems," *Autonomous Robots*, vol. 41, no. 4, pp. 1027–1046, 2017.